Thermal Fatigue Cracking of an IM7/5250-4 Cross Ply Laminate: Experimental and Analytical Observations

RICHARD W. DALGARNO
Firehole Technologies Inc., Laramie, Wyoming 82071, USA

MARK R. GARNICH*
Department of Mechanical Engineering, University of Wyoming
1000 E. University Ave., Laramie, Wyoming 82071, USA

ERIK W. ANDREWS
Firehole Technologies Inc., Laramie, Wyoming 82071, USA

ABSTRACT: Coupons of a balanced and symmetric cross ply laminate with polished edges made from IM7/5250-4 were thermally cycled between room and liquid nitrogen temperatures to induce cracks in the matrix. Edge crack densities for each symmetric lamina pair were recorded as a function of the number of cycles. Coupons with an epoxy coating on the polished edges experienced minimal cracking in all interior plies compared to significant cracking for uncoated specimens. This suggests that edge effects play a dominant role in crack initiation. Crack counts were quite different than recorded by another research group for nearly identical tests. Thermal shock was eliminated as a possible significant contributor to the overall physics driving crack formation. Stress analysis was used to support discussions that explain some of the observed trends in crack densities in the various ply pairs. The number of thermal cycles reached 2600 without a clear indication of crack saturation in any of the plies.

KEY WORDS: cryogenic, matrix cracking, cross ply, composite.

INTRODUCTION

CARBON FIBER REINFORCED plastic (CFRP) materials are currently being studied for application in reusable launch vehicles (RLV). In particular, they may be well-suited for linerless storage and transportation of cryogenic fluids. The main benefit of using

*Author to whom correspondence should be addressed. E-mail: garnich@uwyo.edu
Figures 1 and 2 appear in color online: http://jcm.sagepub.com

0021-9983/09/23 2699–17 $10.00/0 DOI: 10.1177/0021998309345315

composites for RLV is the reduction in structure weight due to their high-specific strength and stiffness when compared to metals. A study by Kessler [1] found that replacing a traditional fuel vessel with one made entirely from composites would reduce the tank weight by 40% and the overall vehicle weight by 14%. This reduction in weight would lead to significant cost savings over the lifetime of the RLV. However, composites are prone to certain types of damage. The environment of space can subject materials to large cyclic temperature variations that can result in considerable thermal stress and damage. For instance, during re-entry into earth's atmosphere, the tanks, which are originally at the temperature of the cryogenic fluid ($\approx -196^{\circ}$C for nitrogen, $\approx -253^{\circ}$C for hydrogen), can reach temperatures of above 127°C [1]. Materials may also be subject to varied levels of solar radiation when they are directly in view of the sun and when they are shadowed. Tank materials also undergo thermal cycles during cryogen filling and draining.

One adverse effect of thermal cycling and associated thermal-stress cycling in composites is microcracking at the ply level, which is illustrated in Figure 1. Microcracking consists of cracks that typically span the thickness of the lamina and run parallel to the fibers. Cracks occur in the matrix and the fiber-matrix interface and can lead to dimensional instability, gas-leakage paths, and the alteration of effective laminate material properties such as strength and stiffness. Crack induced leakage paths are particularly of interest to fuel tanks because these paths may allow for unacceptable loss of fluid that could compromise expensive missions in space.

The cause of microcracking is primarily due to stresses resulting from the mismatch in coefficients of thermal expansion (CTE) at both the ply level (macro) and fiber-matrix level (micro). When a cross-ply laminate is exposed to a large temperature decrease relative to its stress-free temperature, the mismatch in CTE between orthogonal plies results in significant transverse tensile normal stress and longitudinal compressive stress in each ply. The in-plane transverse tensile stresses are most significant with regard to ply cracking since, for large temperature changes, they can approach and exceed the transverse tensile strength of the ply.

At the fiber-matrix level, concentrations of shear stress as well as tensile normal (peel) stress can occur at the fiber–matrix interface in the region local to the geometric discontinuity, where the fibers terminate at ply free-edges. Local fiber–matrix interface failure

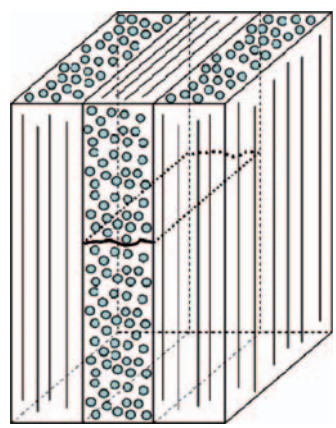

Figure 1. *Transverse microcrack in a cross-ply laminate.*

creates initiation sites for through ply cracks in the presence of ply level transverse tensile stresses. Through-thickness cracks form and propagate through the matrix parallel to the fibers as a result of cyclic thermal stress (thermal fatigue).

Numerous investigations have been conducted in an attempt to gain experimental evidence regarding factors that influence microcracking, e.g., [2–12]. The majority of cryogenic thermal cycling research is performed using flat laminate coupons, which have their edges, and hence the fibers ends, directly exposed (such edges are referred to here are free-edges). In a fuel tank or pressure vessel, true free-edges usually will not be present. Such fuel tanks are typically fabricated using the filament winding method, which uses continuous fibers. These fibers must eventually terminate, but the fiber ends are generally not directly exposed. Rather, they are embedded or potted in the matrix material. Accordingly, testing free-edge coupons may not be the best approach for studying damage mechanisms in storage tanks. They are, however, an economical means to further understand microcracking and qualitatively compare different material systems for their relative resistance to microcracking.

A situation that more closely resembles the configuration of fiber ends in pressure vessels is achieved by applying a thin layer of epoxy to the coupons edges, which effectively embeds the fiber ends in epoxy. To date, the authors are unaware of any previous studies where embedding the edges in epoxy prior to thermal cycling was investigated. Here, coupons with free-edges and capped-edges were thermally cycled between room temperature and cryogenic temperature to help judge the influence of free edges on the thermal fatigue process.

Also considered in this study are the effects of a thermal gradient in the coupon caused by the high rate of heat transfer from the coupon to the cryogenic fluid during rapid submersion. To achieve this, free-edge coupons were subjected to a thermal cycle that allowed them to be slowly cooled before submersion in liquid nitrogen, thus reducing the thermal gradient. Some results from a companion micromechanical modeling study are used to help understand the microscale stresses that occur at the free edges. In addition, a thermal shock finite element model was developed to understand thermal shock effects.

EXPERIMENTAL

Material

A CFRP composite material, IM7/5250-4, was used to fabricate all of the laminates. The IM7 fibers are continuous, PAN based, intermediate modulus fibers manufactured by Hexcel. The matrix material, 5250-4, is a high temperature bismaleimide resin with a continuous service temperature range up to 204°C, made by Cytec Engineered Materials. The prepreg resulted in an average ply thickness of 0.14 mm and a fiber volume fraction of 60%. The thermoelastic properties used for the finite element model were published by Kim and Castro [13] and Kim et al. [11] for unidirectional IM7/5250-4 lamina and are shown in Table 1. Note that the transverse shear modulus and ν_{23} values were only available for 23°C, and it was assumed that these values do not vary with temperature.

All tests were performed on a cross-ply, symmetric lay-up, $[0/90]_{2s}$, resulting in a laminate thickness of ~ 1.12 mm. Plies within this symmetric laminate are referred to in pairs, where pair 1:8 are the outer plies and pair 4 : 5 are the block ply pair in the center of the laminate. A heated platen press in combination with a custom-built flat aluminum

chamber was used to vacuum bag and cure the laminates according to the manufacturer's specifications. This device is similar to an autoclave, but is suited for use in a heated mechanical press. Coupons were cut from the cured plate and the edges polished in a series of steps that ended with the use of 0.05 μm alumina slurry. The coupons were then ultrasonically cleaned and rinsed with distilled water to remove debris. This resulted in a mirror finish suitable for viewing cracks with an optical microscope. The coupons were cut into two sizes: 152 mm × 15.2 mm for the 'free-edge' experiments and 73 mm × 15.2 mm for all other experiments.

Cryo-cycler

To facilitate thermal cycling of coupons in liquid nitrogen an automated system was designed and built based on a similar device described in the literature [4–6]. A photo of the system is shown in Figure 2. In operation, a coupon basket is lowered into a dewar

Table 1. Thermoelastic properties of IM7/5250-4 unidirectional lamina.

Temperature (°C)	−196	23	150
Longitudinal Modulus, E_1 (GPa)	174	172	172
Transverse Modulus, E_2 (GPa)	12.1	10.5	9.9
Shear Modulus, G_{12} (GPa)	9	5.5	4.8
Transverse Shear Modulus, G_{23} (Gpa)	3.3	3.3	3.3
Poisson's ratio, ν_{12}	0.36	0.36	0.36
Poisson's ratio, ν_{23}	0.56	0.56	0.56
Longitudinal CTE, α_{11} (10^{-6}/°C)	0.25	0.25	0.25
Transverse CTE, α_{22} (10^{-6}/°C)	21.1	24.7	24.7

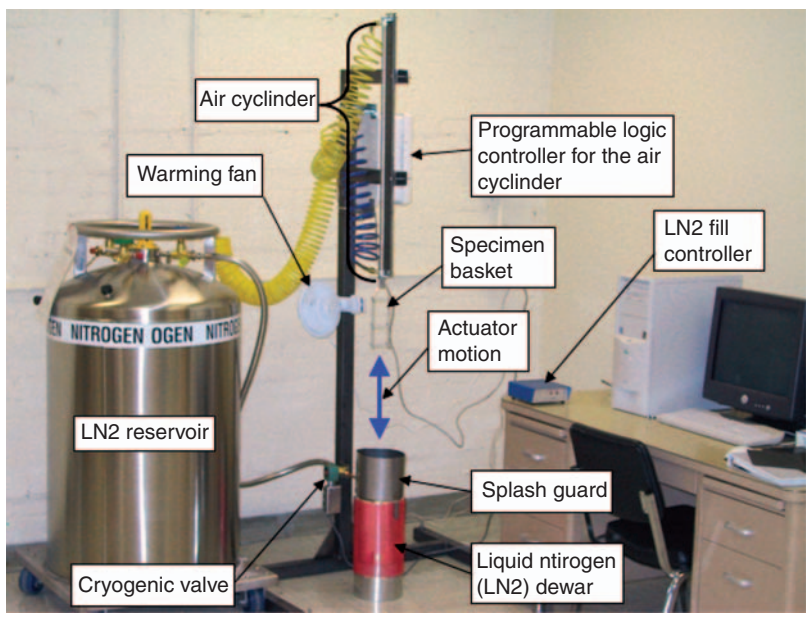

Figure 2. *Cryogenic cyclic material testing apparatus.*

containing LN_2 using a double-acting air cylinder activated by an air solenoid valve. When the basket is retracted, ambient air is forced over the coupons by a small fan to accelerate the warming and shorten the total cycle time. The air solenoid valve is controlled via a programmable logic controller. The LN_2 level in the small dewar was maintained using a LN_2 level sensor and controller and was supplied by a 230 liter reservoir. This system allowed up to 500 continuous cycles unattended before the LN_2 reservoir was depleted. The cryo-cycler was subsequently modified by substituting a three-way air cylinder in place of the two-way cylinder for the reduced thermal shock experiment. The three-way cylinder allowed a delay just above the LN_2 to allow for slower cooling of the coupons in the cold gas just above the liquid.

Crack Density Measurement

An optical microscope was used at 200 × magnification to inspect the polished edges for cracks. An initial inspection was made prior to thermal cycling to ensure the coupons were free of cracks. Once the experiments began, periodic counting of cracks on all coupons was performed. Cracks were counted on the long edge of the coupons and for a crack to be counted it had to span the full thickness of the ply. The reported crack densities are averages of those found in ply pairs that are symmetric about the mid-plane of the 8-ply laminate. For example, the crack density for plies 2 and 7 were averaged. The crack density (ζ) was determined here according to Equation (1) where N is the total number of cracks counted in a batch of n coupons and l is the length of the test section for a ply pair.

$$\zeta = \frac{N}{n(2l)} \tag{1}$$

Hence, ζ is the lineal crack density per ply within a ply pair as observed on the coupon edges. A photomicrograph of a typical microcrack is shown in Figure 3.

The coupon size varied depending on the experiment. For the free-edge experiment, long coupons were used while shorter coupons were used for capped-edge and reduced-shock

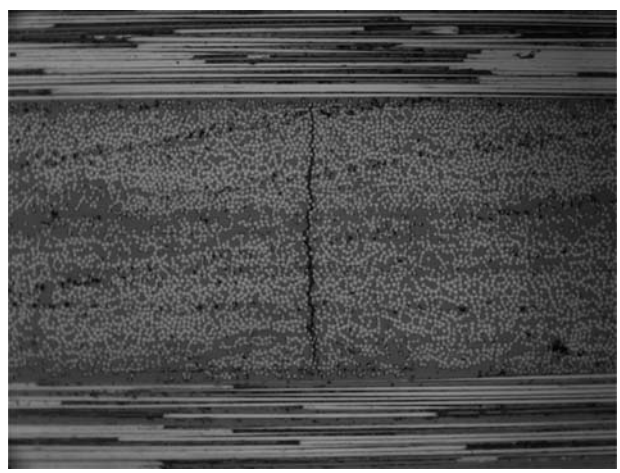

Figure 3. *Photomicrograph of a typical microcrack.*

experiments. In order to avoid potential end effects, crack counts were restricted to a test section in the middle of each coupon. The test sections measured 50 and 34 mm, respectively, for the long and short coupons. Since the test section was on the long side of the coupons, two coupons cut orthogonal to each other were required to expose cracks on the long edges for all symmetric ply pairs of the cross-ply laminate.

Description of Experiments

Three experiments were conducted and all involved thermal cycling from room temperature ($\sim 23^{\circ}$C) to LN_2 temperature (-203°C at the test elevation of 2200 m.). For the first experiment, referred to as the free-edge experiment, 10 coupons with free-edges were cycled 2600 times with crack inspection after 0, 1, 5, 30, 75, 125, 175, 250, 325, 400, then every 100 until 1000 total cycles and then every 400 until 2600 cycles. Following the procedure described by Bechel et al. [4], each cycle consisted of a hold time of 2 minutes in LN_2 followed by a 10 minutes hold in front of a fan at room temperature. They determined this cycle by embedding a thermocouple inside a coupon and measuring the time required to come within 5°C of the desired temperature extremes. They added time to each step to be conservative. The purpose of this experiment was to provide baseline data that can be used for comparison with experiments that followed as well as for comparison with data collected by others. Also, this data was intended to help determine the crack density saturation for this particular laminate subject to thermal cyclic loading only.

Due to the length of the specimens and limitations of the available microscope, it was not possible to examine the short ends under a microscope without cutting the samples into smaller lengths. Therefore, the only opportunity to examine the ends was after the 2600th cycle. At this point, the ends were cut, polished, and examined for cracks to see if there was a difference in the short edge vs. long edge crack densities. Unfortunately the ends were not polished prior to thermal cycling so they differed from the long edges in that respect.

The second experiment, referred to as the capped-edge experiment, was identical to the free-edge experiment except it included only 1600 thermal cycles and the polished coupon edges were coated in a layer of epoxy. In these tests the edges were inspected for cracks every 100 cycles. In preparation for coating with epoxy the coupon edges were first polished and cleaned as discussed earlier. Next, masking tape was applied to all surfaces of the coupon except the edges. The epoxy was then painted on the edges and left to dry at room temperature overnight. The tape was then removed, and the epoxy was cured in an oven. Preliminary tests involving 600 cycles in LN_2 showed that the epoxy stayed securely bonded to the edges. As described earlier, two coupons cut orthogonal to each other were required in order to get a full crack count for all ply pairs. Since the edge epoxy had to be removed in order for the cracks to be visible under a microscope, it was not possible to count cracks on a single set of coupons for the duration of the experiment. Thus, at the completion of every 100 cycles, four coupons (2 sets of 2 samples of each orientation) were extracted, the edge epoxy was removed using sandpaper, and the edges were re-polished. After the cracks were counted on these specimens, they were no longer cycled since the edge epoxy had been removed. This procedure required 64 coupons (16 counts $\times$ 4 coupons/count) altogether.

For the third experiment, referred to as the reduced-shock experiment, eight free-edge coupons were cycled between ambient conditions and LN_2, with the addition of an intermediate cooling period above the surface of the LN_2 prior to fully submerging the coupons.

In order to establish a cooling period, the temperature of the column of nitrogen gas inside the dewar above the liquid surface was first measured to be −170°C. A thermocouple was then taped between two coupons and lowered to within 1–2″ of the liquid surface. After 4 minutes, the thermocouple temperature was −168°C. Based on this, a conservative time of 6 minutes was chosen for the cooling period in the gas. A full cycle began with 6 minutes of cooling above LN_2, followed by a 2 minutes submersion, and finished with a 10 minutes warm up at room temperature in front of the fan. Cracks were counted after 30, 75, 125, 175, 250, and 325 cycles. The decision to discontinue the experiment at 325 cycles will be discussed in the results section. This cooling in gaseous LN_2 allows for a less severe temperature gradient due to the decreased rate of heat transfer in gas compared to liquid.

THERMAL SHOCK FINITE ELEMENT MODEL

A large through-thickness temperature gradient is formed in a coupon when it is initially plunged into LN_2. When the coupon is first submerged, the outer surfaces are in direct contact with the boiling LN_2 and rapidly lose heat, while the inner volume of the coupon remains at a relatively higher temperature for a short period of time. Such a gradient would typically induce significant thermal stresses that are larger than the thermal stresses in a uniformly cooled coupon. An extreme (conservative) thermal gradient can be simulated by assuming the outer ply temperature equal to the LN_2 temperature, while maintaining all inner plies at room temperature. A model that simulates this 'worst-case' scenario was developed and the resulting transverse stresses were compared to the stresses from a model that had a uniform laminate temperature. The dimensions of the model were based on the dimensions of the small experimental coupons, which were 73 mm long and 15.2 mm wide with a thickness equal to 1.12 mm. Since the coupons have three planes of symmetry, the model was constructed using only an eighth of the volume of the real coupon. This symmetric model used symmetry boundary conditions on the three 'cut' symmetry surfaces to accomplish this and the resulting dimensions were $36.5 \times 7.6 \times 0.56$ mm. Three-dimensional rectangular 20-node quadratic continuum finite elements were used.

A view of a corner of the model with the applied temperature field is shown in Figure 4. The temperature of the upper layer of elements in ply 2 is −86.5°C, which is the average of the temperatures of the nodes above and below this layer of elements. While this is not the most extreme thermal gradient possible, it does still simulate a severe thermal gradient.

STRESS-FREE TEMPERATURE DETERMINATION

In order to predict realistic thermal stresses using the finite element model, an estimate of the laminate stress-free temperature was necessary, where the stress-free temperature is the temperature at which ply level thermal stresses are zero in the laminate. Residual stresses in unsymmetric laminates will cause out-of-plane deformation known as warpage or curvature. Depending on the lay-up, an unsymmetric laminate will be flat at the stress-free temperature and saddle shaped, as predicted by CLT, at lower temperatures. This prediction was found to be incorrect for thin laminates, however, by Hyer [14] who found that the cured shapes of thin unsymmetric laminates actually form into part of a right circular cylinder upon curing. Such laminates undergo bifurcation, which happens when the saddle shape solution becomes unstable and transforms into one of two possible stable cylindrical shapes via a snap-through action [15]. The use of classical lamination theory to predict this

curvature was found to be acceptable by Hamamoto and Hyer [16] who found errors of $< 5\%$ between measured curvatures and those predicted by CLT for thin laminates.

The measurement of residual stresses can be accomplished using a number of methods such as photo-elasticity, embedded strain gauges, and interferometry [17]. Destructive techniques, such as first-ply failure and stress–relaxation based methods, can also be used. One of the most elementary approaches is the measurement of the curvature of unsymmetric laminates. The most common approach is to cut the laminate into thin strips, trace the curvature, and measure the center deflection h and chord length $2L$. The associated geometry is illustrated in Figure 5. Strips are used instead of the whole laminate for ease of measurement.

Assuming the traced curve is a section of a circle, a simple derivation yields the curvature κ as the inverse of the radius of curvature ρ to be:

$$\frac{1}{\kappa} = \rho = \frac{1}{2}\left(\frac{L^2}{h} + h\right) \tag{2}$$

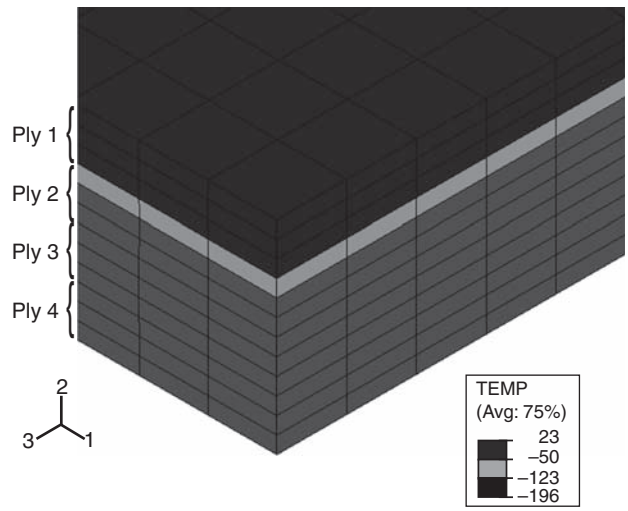

Figure 4. *Applied temperature field for the thermal shock model.*

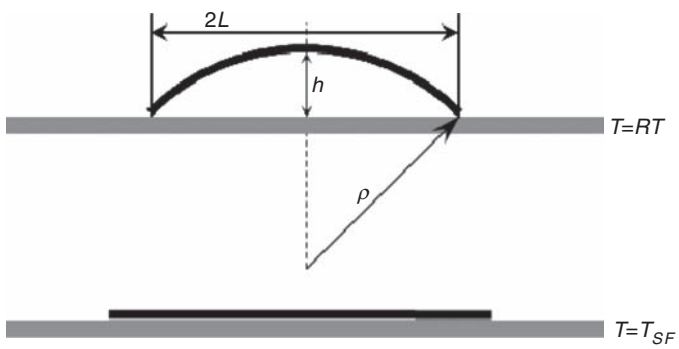

Figure 5. *Unsymmetric laminate warpage and geometry.*

With the estimated curvature known, CLT can be used to solve for the stress-free temperature.

The stress-free temperature of unsymmetric laminates can also be approximated using a simple experimental method. As stated before, when the laminate is flat, it is at the T_{SF}. Based on this, a laminate strip can be placed on top of a flat plate in an oven with a clear viewing window and the temperature can be slowly increased until the strip lays flat on the plate. The shapes of the strip at room temperature and at the stress-free temperature are shown in Figure 5.

RESULTS

Free-edge Coupons

The microcrack density as a function of the number of thermal cycles for the free-edge coupons is shown in Figure 6. All plies resisted cracking until after 30 cycles, with ply pair 3:6 resisting until after 1000 cycles. Generally, all plies except 3 and 6 had significant cracking after 175 cycles. Although it was hoped that saturated edge crack densities would be reached, it appears in Figure 6 that saturation has not been reached in any of the plies though partial leveling of some curves occurred at the end of the test.

The differences in the crack densities between different ply pairs can be partially explained by the effective crack width as it is known that thin plies can experience higher crack densities due to the smaller zone of stress relief around the narrower cracks. With this in mind it is notable that the block ply pair 4:5 is effectively double the thickness of the ply pairs 2:7 and 3:6, thus producing cracks twice as wide. Also, cracks in the surface plies 1:8 are half cracks so the effective crack width in those plies is double the width compared to cracks in ply pairs 2:7 and 3:6. This provides some basis for the lower densities observed in ply pairs 4:5 and 1:8 compared to pair 2:7. One would expect that the crack densities in ply pairs 2:7 and 3:6 would be similar, given that they are the same thickness and since the laminate was symmetric, balanced, and contained no angle plies.

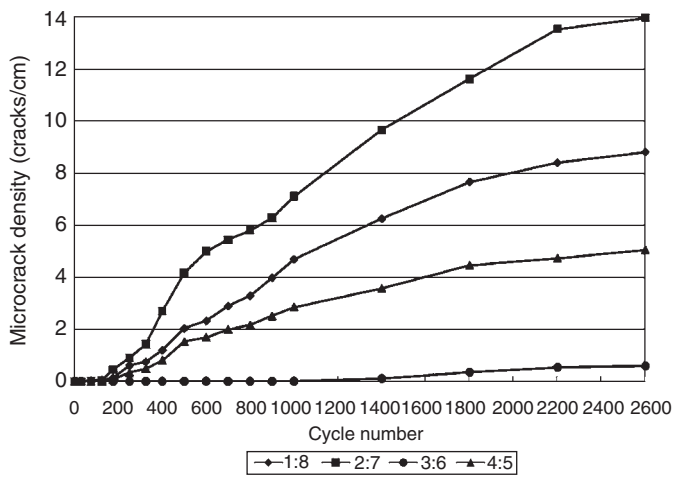

Figure 6. *Free-edge microcrack density by ply pair vs. cycle number.*

Further, according to a laminate analysis these ply pairs should see the virtually the same stress state. As Figure 6 shows, however, ply pair 3:6 had the lowest crack density while pair 2:7 had the highest density. The reasons for this difference are not known. Only the transient thermal load was suspected as a possible contributor to the different crack counts observed for these two ply pairs. This motivated the reduced thermal shock experiment discussed later.

The present results for ply pairs 4:5 and 2:7 differ considerably from results reported by Bechel and Kim [5] who tested the same material and lay-up, but used samples that measured 50.8×50.8 mm, to 1000 cycles. They reported that only the outer plies 1:8 had significant cracking, with sparse cracking of all inner plies. A comparison with the first 1000 cycles of the free-edge tests is shown in Table 2.

Some small error may be present in the values from Bechel and Kim in Table 2 since they were estimated from graphs. The most obvious difference is the almost complete lack of cracks in the Bechel and Kim data for all interior plies including the block ply pair 4:5 after 1000 cycles. Whereas, the present tests produced significant crack densities in interior ply pairs 4:5 and 2:7 after only several hundred cycles. It is possible that this disagreement can be attributed to differences in how the laminates were laid-up and cured and differences in the test environment, particularly the humidity level. One theory was that a higher humidity environment will help suppress crack initiation because the swelling of the matrix around the fiber ends suppresses crack initiating interaction stresses between fiber and matrix. It is believed that the environment Bechel and Kim tested in had a higher humidity. This idea is partially confirmed by pictures published in Bechel et al. [18], which show considerable frost buildup on the mouth of a LN_2 dewar. In the tests conducted here there was little or no frost buildup in any of the tests. The effect of moisture in these tests is the subject of ongoing work. Two common trends between the two sets of data are a lack of cracks in ply pair 3:6, and similar crack densities in the outer plies 1:8 after 1000 cycles.

Table 3 shows the crack densities at 2600 cycles, as counted on the long (152 mm) and short (15.2 mm) sides of the specimens. The outer ply densities remained unchanged, but all of the inner plies had considerably different densities. These differences remain unexplained although, unlike the long edges, the short edges were not polished prior to thermal cycling. As is illustrated later, the microstresses local to the fiber ends of a polished edge

Table 2. Ply-by-ply crack density (cracks/cm) vs. cycle number.

	Bechel and Kim data				New data			
Cycle	**1:8**	**2:7**	**3:6**	**4:5**	**1:8**	**2:7**	**3:6**	**4:5**
0	0	0	0	0	0	0	0	0
30	0	0	0	0	0	0	0	0
75	<0.1	0	0	0	0.04	0.02	0	0
125	<0.1	0	0	0	0.06	0.05	0	0
175	<0.1	0	0	0	0.14	0.44	0	0.07
250	0.1	0	0	0	0.61	0.91	0	0.34
325	0.2	0	0	0	0.75	1.43	0	0.49
400	0.35	0	0	0	1.2	2.71	0	0.81
500	0.9	0.05	0	0	2.03	4.16	0	1.53
650	2.25	0.08	0	0	2.61	5.22	0	1.85
800	3.8	0.08	0	0	3.29	5.81	0	2.17
1000	5.9	0.16	0	0.07	4.69	7.11	0	2.85

are significant and would clearly be different than for an unpolished edge. Another obvious difference is that the short edges are an order of magnitude smaller than the long edges. However, they are still long compared to the ply (0.14 mm) and laminate (1.12 mm) thicknesses. There is certainly a statistical issue since a single crack in a ply pair on the short edge of a single coupon corresponds to a crack density of 0.33 cracks per centimeter making the difference shown in Table 3 for ply pair 3:6 statistically insignificant.

Capped-edge

The edge microcrack density vs. number of cycles for the coupons with their laminate edges coated in epoxy is compared with the data from the free-edge coupons in Figure 7 excluding pair 3:6 where there were almost no cracks in either test. Note that the free-edge coupons are represented by the solid symbols and are labeled 'free' in the figure legend. It is notable that all capped-edge plies were crack free until after 200 cycles and that cracking was effectively suppressed in all interior plies. The highest edge crack density among all interior ply pairs was very low at 0.15 cracks/cm. It should be kept in mind that unlike the free-edge specimen data, each data point for the capped-edge data was from a different group of four coupons as opposed to updating the crack counts over and over again on the same coupons as was the case with the free-edge experiment.

In Figure 7 it is clear that 'eliminating' free-edges drastically reduces the edge crack density of all inner plies. However, the capped-edge outer ply crack density, though

Table 3. Microcrack densities for the long and short sides at 2600 cycles.

	Ply pair			
Edge	**1:8**	**2:7**	**3:6**	**4:5**
Long	8.8	13.95	0.59	5.04
Short	8.86	3.15	0	0

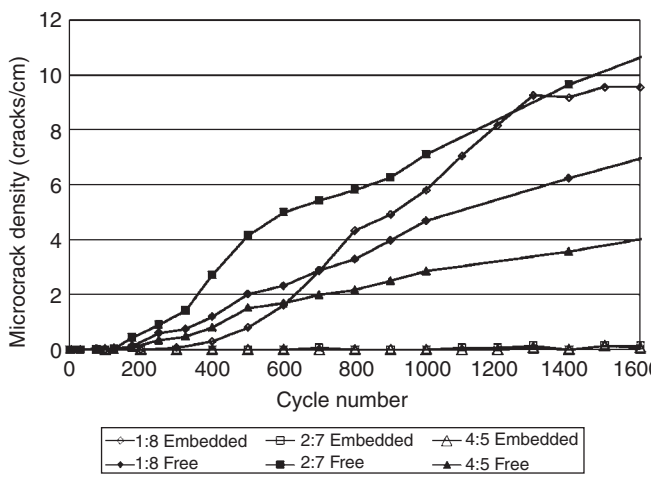

Figure 7. *Capped-edge and free-edge microcrack density by symmetric ply pair vs. cycle number.*

initially lower, rapidly caught up to and exceeded that of the corresponding plies in the free-edge experiment. The rate of new crack formation in the outer plies of the capped-edge coupons slowed down considerably after 1300 cycles, which suggests that the crack density was approaching a saturation point of around 10 cracks/cm. There is some evidence to support this hypothesis in Figure 6 where an extrapolation of the curve for ply pair 1:8 with free-edges would also suggest a saturated density of about 10 cracks/cm. However, Bechel and Kim [5] achieved a crack density of 16 cracks/cm for the same ply pair after 1000 cycles. One possible explanation would be the presence of delaminations as a secondary damage mechanism enhancing the stress relief around the cracks. However, no delaminations were observed in these experiments.

Reduced-shock

The microcrack density vs. cycle number for the reduced shock and free-edge experiments are compared in Figure 8. Again, the free-edge data points are marked 'free' in the figure legend. Outer ply cracking initiated after 125 cycles for the reduced shock coupons, but by 250 cycles, the edge crack density surpassed that of the free-edge (full shock) coupons. In both experiments, cracking in the ply pair 2:7 was first observed after 75 cycles and both trends followed similar trajectories. For the block ply pair 4:5, the reduced shock coupons experienced slightly less frequent cracking than free-edge coupons and these cracks initiated later as well. No cracking was seen in plies 3 and 6 through 325 cycles for both experiments. The overall trend is similar for the free-edge experiments in that the outer plies develop cracks earlier and more frequently than the interior plies. Based on these results, it appears that reducing the thermal gradient does not significantly change the number or distribution of cracks in this laminate. This observation led to the termination of the reduced shock experiment after only 325 cycles.

The basic mechanics of the thermal stress problem also support this conclusion. If one considers the very stiff fibers with slightly negative axial CTE which yields a very low

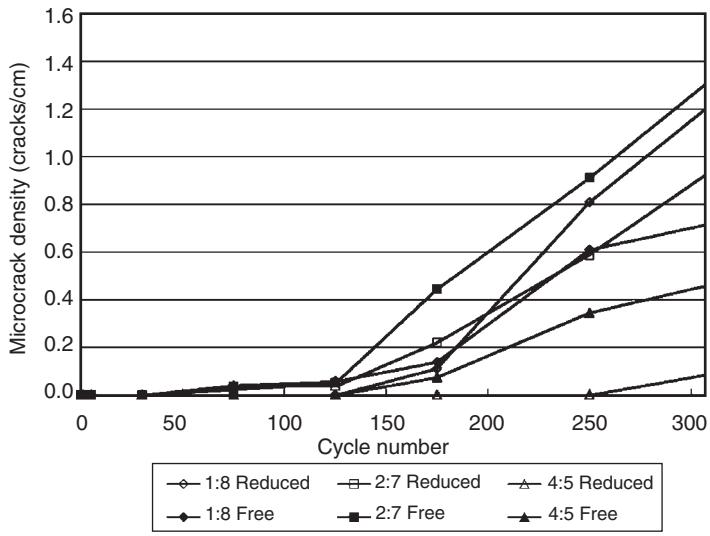

Figure 8. *Reduced shock and free-edge microcrack density by symmetric ply pair vs. cycle number.*

lamina axial CTE, then the laminate has a very low in plane CTE. The transverse tensile stress develops because the transverse ply CTE is large, but the stiff fibers in adjacent plies prevent the thermal contraction. Therefore, the deformation of the laminate and the peak internal ply stresses are almost the same for both the slow and fast cooling scenarios. Since the stresses are insensitive to the cooling rate it is expected that the thermal fatigue related cracking would be similar as verified by the experimental data displayed in Figure 8.

Thermal Shock Finite Element Predictions

The laminate $[0/90]_{2s}$, with all of its plies at LN_2 temperature was modeled and the magnitude of the peak transverse stresses in the bulk was found to be ~ 100 MPa. The model was then modified so that the temperature of all inner plies was equal to room temperature, while the outer ply remained at LN_2 temperature. The resulting magnitude of the peak transverse stresses in the bulk was found to be ~ 105 MPa. Thus, a worst-case thermal gradient will increase the peak transverse stress by only 5%. These modeling results support the minor differences observed between the free-edge and reduced-shock experimental results.

Stress-free Temperature Determination

The stress-free temperature used in the models was determined based on the average of two techniques. Heating an unsymmetric, $[0/90]_4$, laminate strip in an oven until it was no longer warped resulted in a stress-free temperature of 225°C. Tracing the curvature of the same strip and using CLT yielded a stress-free temperature of 204°C. Thus, the stress-free temperature used in the finite element models was 214°C. It should be noted that this experimentally determined value is close to the post-cure temperature of 226°C, which is often assumed to be the stress-free temperature.

Micromechanics

In a related study [19] performed in conjunction with the present work, a finite element micromechanics model was created to investigate the radial and shear stresses at the fiber–matrix interface near the free-edge of a laminate due to thermal loading. The model is based on a 3D periodic unit cell with hexagonal packing of the fibers. Both bare (fiber ends exposed) and capped (fiber ends coated in a layer of epoxy) models were analyzed and compared. The material modeled was IM7/5250-4 (the same material experimentally tested here) and the fiber volume fraction was 60%. The temperature change (−383°C) applied to the models represents the difference between an estimated stress free temperature (187°C) and the temperature of boiling liquid nitrogen (−196°C). Some of the results from this effort are shown in Figures 9–12. The stresses presented are the combined stresses that arise from the mismatch in CTE between the fiber and matrix and from the ply level transverse tension due to lamina anisotropy. The stresses were taken from an orientation around the fiber perimeter that corresponds to the orientation of the applied transverse tension, which also corresponds to the direction of shortest distance to a nearest neighbor fiber in the assumed hexagonal arrangement. In all plots, the distance along the fiber (horizontal axis in Figures 9–12) is normalized by the fiber diameter and the origin of the horizontal axis corresponds to the end of the fiber. Negative distances correspond to positions inside the epoxy cap. Figure 9 shows the radial stresses

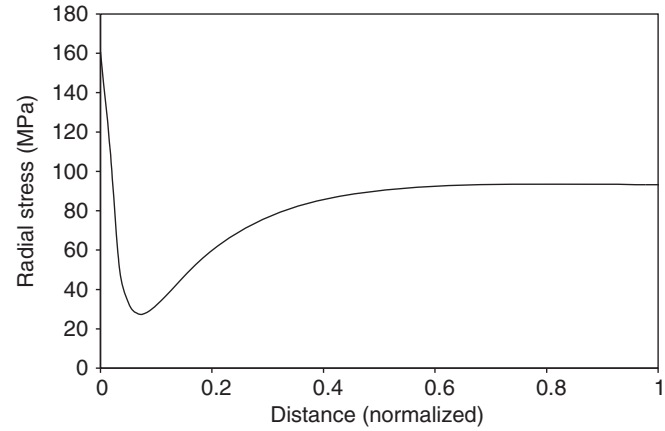

Figure 9. *Radial stresses at the fiber–matrix interface near the fiber end.*

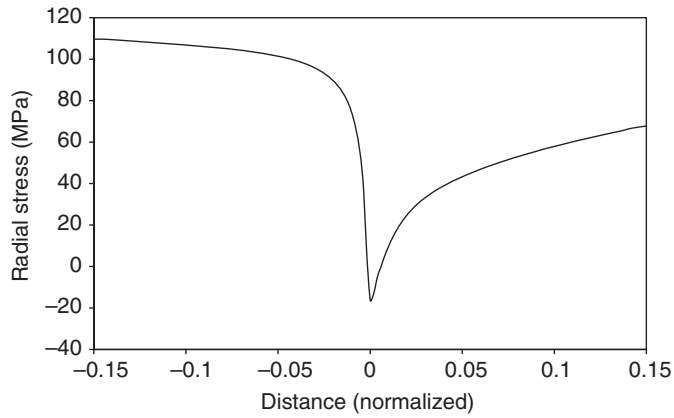

Figure 10. *Radial stresses at the fiber–matrix interface with an epoxy cap.*

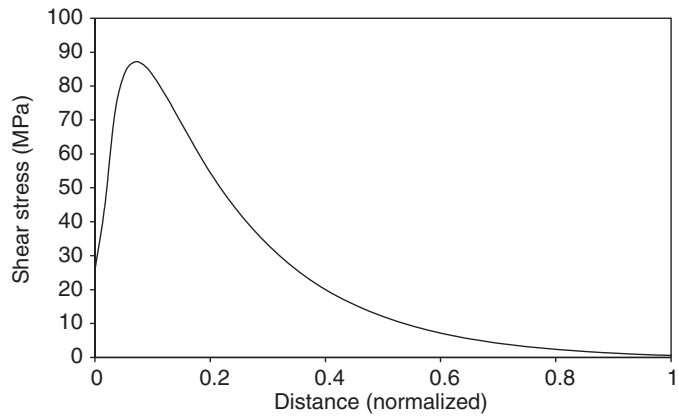

Figure 11. *Shear stress at the fiber–matrix interface near the fiber end.*

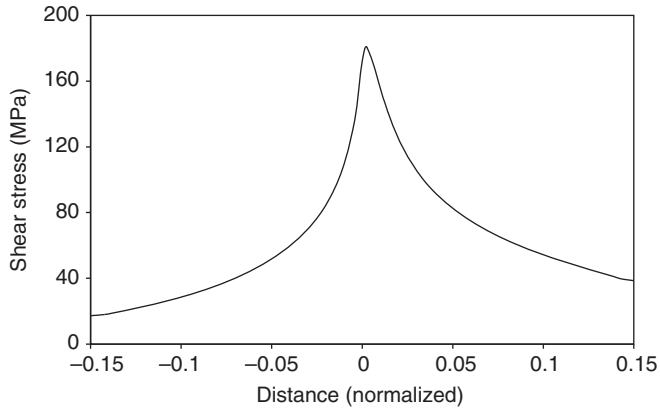

Figure 12. *Shear stresses at the fiber–matrix interface with an epoxy cap.*

at the fiber–matrix interface near the fiber end of a free-edge. Away from the fiber end (in the bulk) the stress is constant, but as the end is approached, the stress decreases then rapidly increases to a tensile singularity at the fiber end. The radial stresses in the vicinity of the fiber end, when an epoxy cap was included in the model, are shown in Figure 10. In this case, the stress singularity is compressive as the fiber end is approached. Thus, the epoxy cap results in a suppression of the tensile singularity at the fiber–matrix interface near the free-edge.

The shear stresses at the fiber–matrix interface for a free-edge are shown in Figure 11. In the bulk, the shear stress is zero, but as the fiber end is approached the shear stress reaches a singularity (peak stress increases without bound as the elements size decreases) just inside the free-edge and returns to zero at the free-edge. The shear stresses with an epoxy cap are seen in Figure 12. The shear stress singularity still exists with a cap and the shear stresses are actually higher for the same finite element mesh density than those of the free-edge model.

The above micromechanics results suggest radial and shear stress singularities exist near the fiber end in the case of a free-edge laminate. These singularities near the fiber end make the fiber–matrix interface a likely candidate for fiber debonding. Consequently, crack initiation is likely to occur at the fiber ends. For the case of a free-edge coated in epoxy, the results indicate a suppression of the tensile radial stress singularity, while the shear stress singularity still exists. These results corroborate with the experimental results in that the embedded-edge experiment showed a significantly lower crack density than the free-edge experiment. This suggests that suppressing the radial stress singularity, despite the presence of a shear stress singularity, will mitigate crack formation.

CONCLUSIONS

An experimental apparatus was built to automatically cycle coupons of a cross ply laminate made from IM7/5250-4 from room temperature to liquid nitrogen temperature. This basic test has been used in the past by others to compare the resistance of various composites to thermal fatigue cracking in the matrix. Matrix edge crack density vs. number of thermal cycles was recorded for a baseline set of coupons, a set of coupons

with an epoxy coating on the edges, and a set of coupons without epoxy that were cooled slowly in gas. Results showed that the epoxy coating nearly eliminated the cracks in all interior plies even after 1600 thermal cycles. Stress analysis from a previous study showed that a tensile stress singularity exists at the fiber–matrix interface at the free edge of the laminate. This singularity was eliminated by the epoxy coating and it was concluded that the free edges play a dominant enabling role in the thermal fatigue cracking of such coupons. The thermal shock associated with plunging the room temperature coupons into liquid nitrogen was verified to have minimal affect on the thermal stresses vs. slow cooled specimens. Experiments confirmed that there was no significant difference between numbers and distributions of cracks for slow cooled vs. thermally shocked specimens.

Two observations remain unexplained and are possible topics for further research. Ply pair 3:6 consistently incurred almost no cracks even for very high numbers of thermal cycles, while neighboring ply pair 2:7 incurred some of the highest edge crack densities. There is no apparent difference between these two ply pairs to explain this difference. For specimens with coated edges the outer ply pair 1:8 experienced significant cracking, while cracking was almost completely suppressed for the interior plies. The outer ply edges may have not been completely coated or the cracks may not originate at the edges for the outer plies. Finally, although coupons were thermally cycled for as many as 2600 times no definitive crack saturation density was achieved in any of the ply pairs. The data does suggest that the outer plies may have a crack saturation density of ~ 10 cracks per centimeter, but this disagrees with results of others where 16 cracks per centimeter were achieved for the same conditions.

REFERENCES

1. Kessler, S.S. (1998). Cryogenic and Mechanical Testing of CFRP for the X-33 LH2 Fuel Tank Structure, Massachusetts Institute of Technology, S.B., TELAC Report no. 98–15.
2. Park, C.H. and McManus, H.L. (1996). Thermally Induced Damage in Composite Laminates: Predictive Methodology and Experimental Investigation, *Composites Science and Technology*, **56**: 1209–1219.
3. Donaldson, S.L. and Kim, R.Y. (2002). Fatigue of Composites at Cryogenic Temperatures, In: *Proceedings of the 47th SAMPE International Symposium*, SAMPE, Long Beach, CA, pp. 1248–1253.
4. Bechel, V.T., Fredin, M.B., Donaldson, S.L., Kim, R.Y. and Camping, J.D. (2003). Effect of Stacking Sequence on Micro-cracking in a Cryogenically Cycled Carbon/Bismaleimide Composite, *Composites: Part A*, **34**: 663–672.
5. Bechel, V.T. and Kim, R.Y. (2004). Damage Trends in Cryogenically Cycled Carbon/Polymer Composites, *Composites Science and Technology*, **64**: 1773–1784.
6. Bechel, V.T., Camping, J.D. and Kim, R.Y. (2005). Cryogenic/Elevated Temperature Cycling Induced Leakage Paths in PMCs, *Composites: Part B*, **36**: 171–182.
7. Lafarie-Frenot, M.C., Hénaff-Gardin, C. and Gamby, D. (2001). Matrix Cracking Induced by Cyclic Ply Stresses in Composite Laminates, *Composites Science and Technology*, **61**: 2327–2336.
8. Lafarie-Frenot, M.C. and Ho, N.Q. (2006). Influence of Free Edge Intralaminar Stresses on Damage Process in CFRP Laminates under Thermal Cycling Conditions, *Composites Science and Technology*, **66**: 1354–1365.
9. Adams, D.S., Bowles, D.E. and Herakovich, C.T. (1986). Thermally Induced Transverse Cracking in Graphite-epoxy Cross-ply Laminates, *Journal of Reinforced Plastics and Composites*, **5**: 152–169.

10. Brown, T.L. and Hyer, M.W. (1996). Effects of Long-term Thermal Cycling on Microcracking Behavior in Composite Materials, In: *Proceedings of the American Society for Composites 11th Technical Conference*, Atlanta, GA, pp. 476–485.
11. Kim, R.Y., Rice, B.P. and Donaldson, S.L. (2002). Microcracking in Composite Laminates under Thermal Environments: 150 to −196°C, In: *Proceedings of the 47th SAMPE International Symposium*, SAMPE, Long Beach, CA, pp. 833–842.
12. Timmerman, J.F., Hayes, B.S. and Seferis, J.C. (2002). Nanoclay Reinforcement Effects on the Cryogenic Microcracking of Carbon Fiber/Epoxy Composites, *Composites Science and Technology*, **62**: 1249–1258.
13. Kim, R.Y. and Crasto, A.S. (1997). Initiation of Free-edge Delamination in a Composite Laminate under Fatigue Loading, In: *Proceeding of the 11th International Conference on Composite Materials*, Gold Coast, Queensland, Australia, pp. 185–193.
14. Hyer, M.W. (1981). Some Observations on the Cured Shape of Thin Unsymmetric Laminates, *Journal of Composite Materials*, **15**: 175–193.
15. Cowley, K.D. and Beaumont, W.R. (1997). The Measurement and Prediction of Residual Stresses in Carbon-fiber/Polymer Composites, *Composite Science and Technology*, **57**: 1445–1455.
16. Hamamoto, A. and Hyer, M.W. (1987). Non-linear Temperature-curvature Relationships for Unsymmetric Graphite-epoxy Laminates, *International Journal of Solids and Structures*, **23**: 919–935.
17. Parlevliet, P.P., Bersee, H.E.N. and Beukers, A. (2007). Residual Stresses in Thermoplastic Composites – A Study of the Literature – Part II: Experimental Techniques, *Composites: Part A*, **38**: 651–665.
18. Bechel, V.T., Negilski, M. and James, J. (2006). Limiting the Permeability of Composites for Cryogenic Applications, *Composites Science and Technology*, **66**: 2284–2295.
19. Andrews, E.W. and Garnich, M.R. (2008). Stresses around Fiber Ends at Free and Embedded Ply Edges, *Composites Science and Technology*, **68**: 3352–3357.